

Misfit layer compounds as ultra-tunable field effect transistors: from charge transfer control to emergent superconductivity

Ludovica Zullo,^{*,†,‡} Giovanni Marini,[¶] Tristan Cren,[‡] and Matteo Calandra^{*,†,‡,¶}

[†]*Department of Physics, University of Trento, Via Sommarive 14, 38123 Povo, Italy*

[‡]*Sorbonne Université, CNRS, Institut des Nanosciences de Paris, UMR7588, F-75252 Paris, France*

[¶]*Graphene Labs, Fondazione Istituto Italiano di Tecnologia, Via Morego, I-16163 Genova, Italy*

E-mail: ludovica.zullo@unitn.it; m.calandrabuonaura@unitn.it

Abstract

Misfit layer compounds are heterostructures composed of rocksalt units stacked with few layers transition metal dichalcogenides. They host Ising superconductivity, charge density waves and good thermoelectricity. The design of misfits emergent properties is, however, hindered by the lack of a global understanding of the electronic transfer among the constituents. Here, by performing first principles calculations, we unveil the mechanism controlling the charge transfer and demonstrate that rocksalt units are always donor and dichalcogenides acceptors. We show that misfits behave as a periodic arrangement of ultra-tunable field effect transistors where a charging as large as $\approx 6 \times 10^{14} \text{ e}^- \text{cm}^{-2}$ can be reached and controlled efficiently by the La-Pb alloying in the rocksalt. Finally, we identify a strategy to design emergent superconductivity

and demonstrate its applicability in $(\text{LaSe})_{1.27}(\text{SnSe}_2)_2$. Our work paves the way to the design synthesis of misfit compounds with tailored physical properties.

The capability of inducing a controlled and tunable number of carriers in few layer systems has been pivotal for the success of 2D materials.¹ However, in metallic few layers 2D dichalcogenides such as NbSe_2 , the largest carrier doping that can be achieved via field effect gating are of the order of $n_e \approx 3 \times 10^{14} \text{ e}^- \text{ cm}^{-2}$,² corresponding to a Fermi level shift of the order of 0.1 eV, too small to drastically change the physical properties.

Recently,³ it has been shown that overcoming this limit is possible in the misfit layer compound (MLC) $(\text{LaSe})_{1.14}(\text{NbSe}_2)_2$, an heterostructure composed of periodically alternating rocksalt monochalcogenide units (RS) and few layers transition metal dichalcogenides (TMDs).^{4,5} In this system, a massive electron transfer from the LaSe RS to the NbSe_2 TMD occurs, leading to a rigid Fermi level shift as large as +0.55 eV. It is, however, unclear if the electron doping in misfits can be in some way controlled by any physical parameter and, more important, how general this mechanism to dope few layer TMDs is.

MLCs have been known for a long time and their structures as a function of the RS and TMD composition have been thoroughly investigated.^{4,5} However, the exploration of physical properties such as Ising superconductivity⁶⁻¹¹ charge density waves (CDW)¹²⁻¹⁶ or topological effects¹⁷ are quite recent. The research in the field has lead to remarkable results but it has mostly proceeded by isolated discoveries and trial and error chemical synthesis, while general rules to understand what happens when assembling different RS and TMDs are missing. The need of a global picture becomes evident when considering that (i) many ternary alloys composed of monochalcogenides can be assembled with practically any few layer dichalcogenide, (ii) the thickness of the dichalcogenide layers can be chosen at will. This makes a lot of possible combinations and leads to many unanswered questions. For example, how does the charge transfer occur in these structures? Are the TMD layers acceptors or donors? How can the charge transfer be tuned? To what extent the electronic structure of the TMD is affected when inserted in the heterostructure? Most important,

what are the emergent properties of the misfit, i.e. properties of the MLC that are absent in the pristine constituents ? How can we design misfit properties from the knowledge of their building blocks ?

In this work we answer these questions by performing extensive first principles electronic structure calculations of MLCs. We identify the fundamental mechanism ruling charge transfer and demonstrate how the charge injection into the TMD layers can be efficiently controlled by chemical alloying in the rocksalt unit. Most important, we show that superconductivity can emerge in MLCs formed by assembling non-superconducting RS and TMDs. Finally, we demonstrate that misfit layer compounds can be assimilated to ultra-tunable field effect transistor with an unequaled charging of the TMD layers. Our work paves the way to extensive experimental synthesis and development of these promising systems.

The chemical formula of MLCs is $(\text{RQ})_{1+\delta}(\text{TX}_2)_m$, where $(\text{TX}_2)_m$ is a m -layers TMD and RQ is a rocksalt monochalcogenide unit (often referred to as Q-layer).^{4,5} Ternary alloys of two monochalcogenides within a single RS Q-layer (e.g. $\text{La}_x\text{Sr}_{1-x}\text{S}$) have also been synthesized¹⁸ leading to MLCs having chemical formulas of the kind $(\text{R}_x\text{M}_{1-x}\text{Q})_{1+\delta}(\text{TX}_2)_m$. As a prototypical example of the MLCs crystal structure we consider $(\text{LaSe})_{1.18}(\text{TiSe}_2)_2$, shown in Fig. 1 (a) and (b). Each TiSe_2 and LaSe sublattice has its own set of cell parameters. Compared to bulk 1TTiSe_2 , the lattice of the TiSe_2 bilayer in the MLC is not perfectly hexagonal and is slightly expanded along one direction. As a consequence, the TiSe_2 sublattice is described by a centered orthorhombic cell with in-plane lattice vectors $\mathbf{a}_1 \approx 3.6 \text{ \AA}$ and $\mathbf{b}_1 \approx 6 \text{ \AA}$. The LaSe sublattice has also an orthorhombic symmetry but with similar in-plane lattice parameters $\mathbf{a}_2 \approx \mathbf{b}_2 \approx 6 \text{ \AA}$. Both systems have the same \mathbf{b} vectors ($\mathbf{b}_1 \approx \mathbf{b}_2$) so that the material is commensurate along this direction. The ratio between the norms of the \mathbf{a}_1 and \mathbf{a}_2 vectors sharing the same direction is an irrational number (see tables in Fig. 1 and 2 in Supplemental Material) making the MLC incommensurate in the \mathbf{a} direction. The mismatch ratio $a_2/a_1 = x/y$ is usually in the range $\sim 1.6 - 1.8$ and sets the parameter δ in the chemical formula through the relation $1 + \delta = 2 \times (a_1/a_2)$. In this work we adopt the

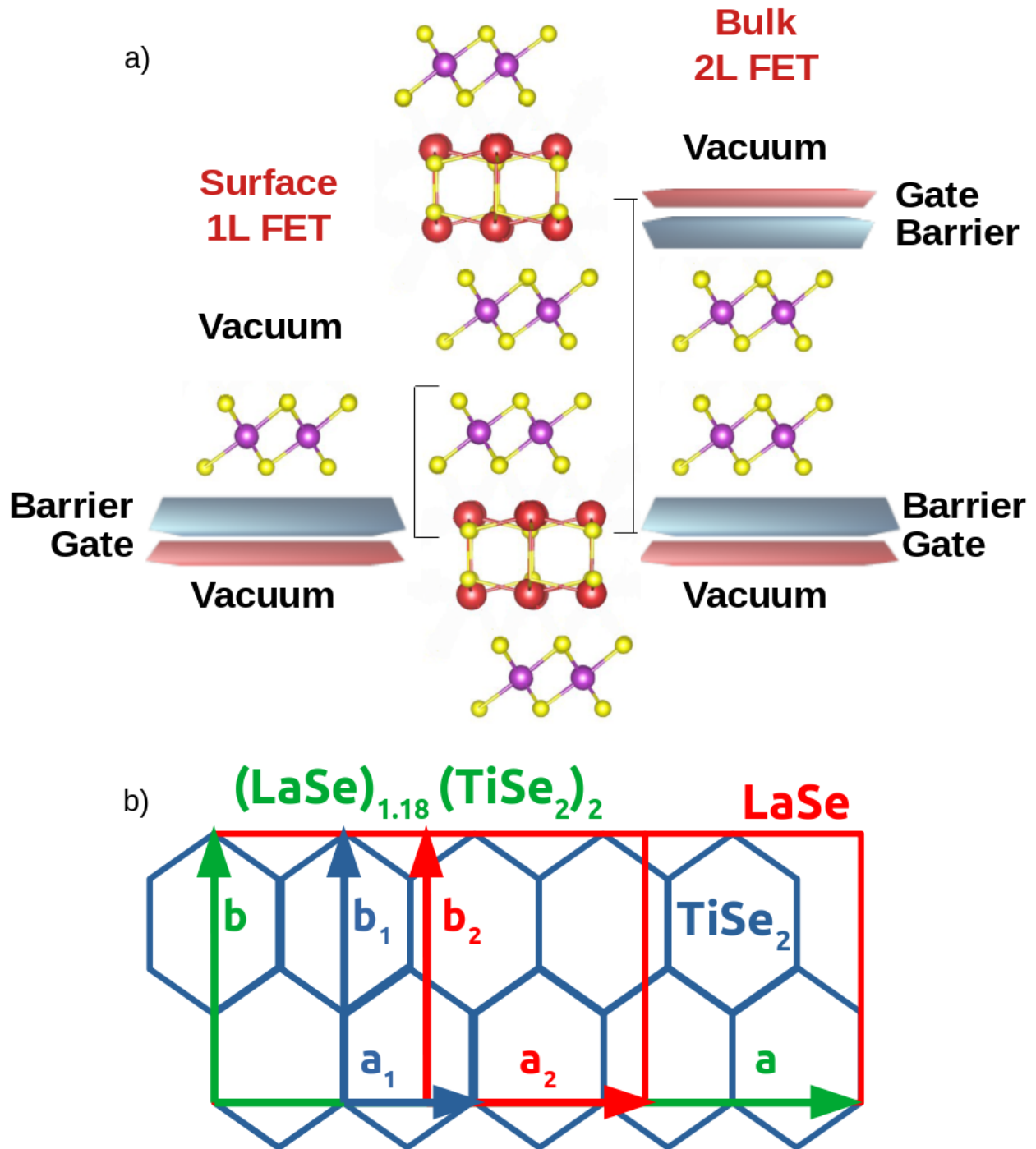


Figure 1: a) Bulk structure of $(\text{LaSe})_{1.18}(\text{TiSe}_2)_2$. The field-effect modeling scheme is depicted for the case of the most common TiSe_2 terminated surface (left) and for bulk TiSe_2 (right). b) Sketch of the unit cell of $(\text{LaSe})_{1.18}(\text{TiSe}_2)_2$ misfit layer compound (\mathbf{a} , \mathbf{b}) compared with the ones of a TiSe_2 monolayer (\mathbf{a}_1 , \mathbf{b}_1) and of a LaSe unit (\mathbf{a}_2 , \mathbf{b}_2).

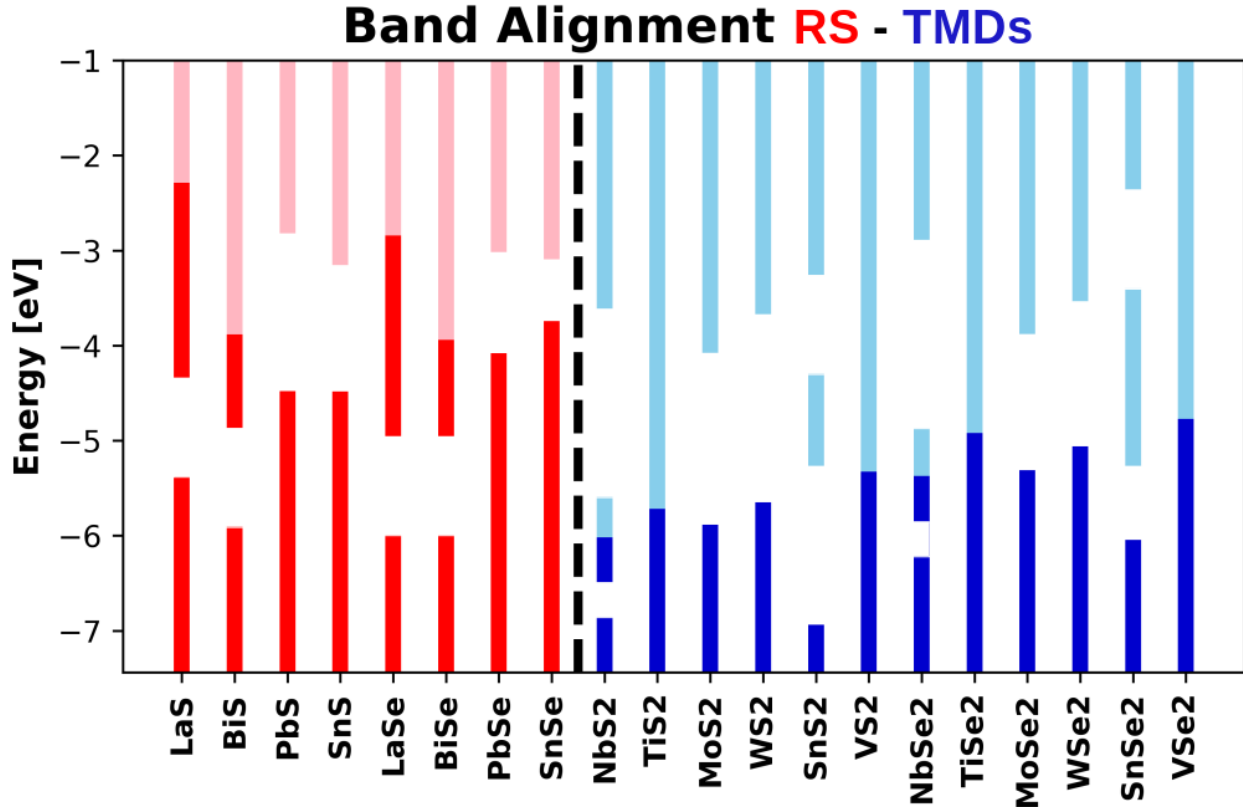


Figure 2: Calculated band-alignment of isolated Q-layer rocksalt structures (red) and single layer transition metal dichalcogenides (blue). Dark (light) bars represents the position of E_F /valence band maximum (E_F /conduction band minimum) for metal/insulators. White spaces in the bars represent gaps in the single particle spectrum. The zero of the energy is set to the vacuum level.

convention of using the value of δ as obtained from the lattice parameters \mathbf{a}_1 and \mathbf{a}_2 of the pristine RS and TMD before assembling them in a MLC structure, as reported in the tables in Figs. 1-2 in the Supplemental Material. The commensurate approximant of each MLCs considered in the current work is reported in Fig. 3 in the Supplemental Material.

The RS layers have a strong intralayer bonding. A strong bonding also forms among the RS and TMDs layers. On the contrary, Van der Waals bonding occurs among the closer TMD layers. After cleavage, for $m > 1$, the surface of the sample is a perfect TMD layer (a single layer in the $m = 2$ case considered in this work ³). In the $m = 1$ case, i.e. a single layer TMD sandwiched among RS Q-layers, the bonding along the z axis is always strong. As a result, the cleavage occurs in-between the RS and TMD bonding and the surface is still

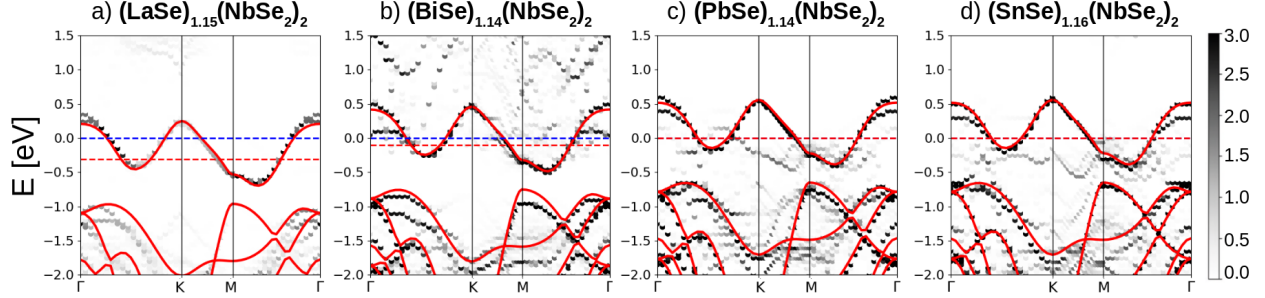


Figure 3: Band unfolding onto the NbSe_2 single layer Brillouin zone for the NbSe_2 misfit series for different rocksalt Q-layers having comparable mismatching ratio close to $7/4$. The band structure for the isolated single layer NbSe_2 (red line) is superimposed and aligned to the Nb d-band in the misfit. The blue dashed line corresponds to the Fermi level E_F of the misfit compound, while the red one to the Fermi level of the isolated NbSe_2 layer. In the last two panels the dashed red line is superimposed to the dashed blue one. Spin orbit coupling is neglected in all the calculations.

a TMD single layer, however it is often less clean and presents several steps and defects.^{6,9} In all cases, there is a substantial experimental evidence³ that ARPES and STS/STM measurements mostly sample the terminating TMD layer without accessing the bulk of the structure. On the contrary, Raman, transport and superconducting measurements probe bulk properties of the crystal.

In order to gain insight on the charge transfer among the RS and TMD layers in the MLC and its relevance for the electronic structure measurements (ARPES), we perform extensive calculations of the work functions of 8 isolated rocksalt Q-layers and 12 isolated TMDs single layers. The choice of considering TMD single layers is motivated by (i) the fact that we consider MLC with $m = 2$ having a single layer TMD as terminating surface and (ii) by the fact that the work functions of bilayers TMDs is fairly close to the one of single layers.¹⁹ Thus, we expect that our results will also hold for the surface and the bulk and for the $m = 1$ case. Calculations are performed with the QUANTUM ESPRESSO²⁰ package and we use the PBE exchange and correlation functional²¹ (see SI for more technical details). Results are shown in Fig. 2.

The key quantities ruling the charge transfer in these systems are the work function difference among RS and TMDs and the consequent band alignment, the lattice mismatching

ratio a_2/a_1 and, finally, the degree of hybridization when the two subsystems are in contact. As shown in Fig. 2, the TMDs globally possess substantially larger work functions than the RS compounds. As the work function is the energy required to transfer an electron from the Fermi level to the vacuum level, RS are always donor and TMDs always acceptors. The net amount of charge transfer depends, however, not only on the work function difference but also on the mutual concentration of the RS and TMD that is related to the mismatching ratio. To explain this more clearly, each RS can transfer a given amount of charge to the TMDs layer, if the mismatching ratio is close to one. However, if the mismatching ratio increases, the relative concentration of RS atoms per TMD cell decreases, and so does the charge transfer. By looking at Fig. 3 in SI, it is clear that the mismatching ratio varies mostly due to the change in the TMD lattice parameter.

In order to demonstrate this global picture we perform explicit calculations for several misfit surfaces terminated by a single layer NbSe_2 but having different RS Q-layers as building blocks and sharing comparable mismatching ratios very close to $7/4$ (these compounds all belongs to the ninth column in the table in Fig. 3 in the Supplemental Material). As it can be seen in Fig. 3, the behaviour of the $(\text{LaSe})_{1.15}(\text{NbSe}_2)_2$, $(\text{BiSe})_{1.14}(\text{NbSe}_2)_2$, $(\text{PbSe})_{1.14}(\text{NbSe}_2)_2$ and $(\text{SnSe})_{1.16}(\text{NbSe}_2)_2$ serie is almost completely characterized by the work function differences. Indeed as $W(\text{LaSe}) < W(\text{SnSe}) < W(\text{PbSe})$, the charge transfer decreases by progressively decreasing the difference $W(\text{NbSe}_2) - W(\text{RS})$, as expected. The work function of BiSe is slightly larger than the one of SnSe, however BiSe seems to transfer few more electrons than SnSe. We attribute this to the metallic character of BiSe and the consequent stronger hybridization occurring between BiSe and NbSe_2 , resulting in a substantial band deformation of the pristine NbSe_2 , as shown in Fig. 3.

Finally we point out that the NbSe_2 electronic structure in going from $(\text{PbSe})_{1.14}(\text{NbSe}_2)_2$ to $(\text{LaSe})_{1.15}(\text{NbSe}_2)_2$ is n-doped rigidly, i.e. the charge transfer simply induces a Fermi level upshift. From this analysis two questions arise: how general is this rigid doping effect and how can it be used to effectively tune the doping? We now show that it is possible to engineer the

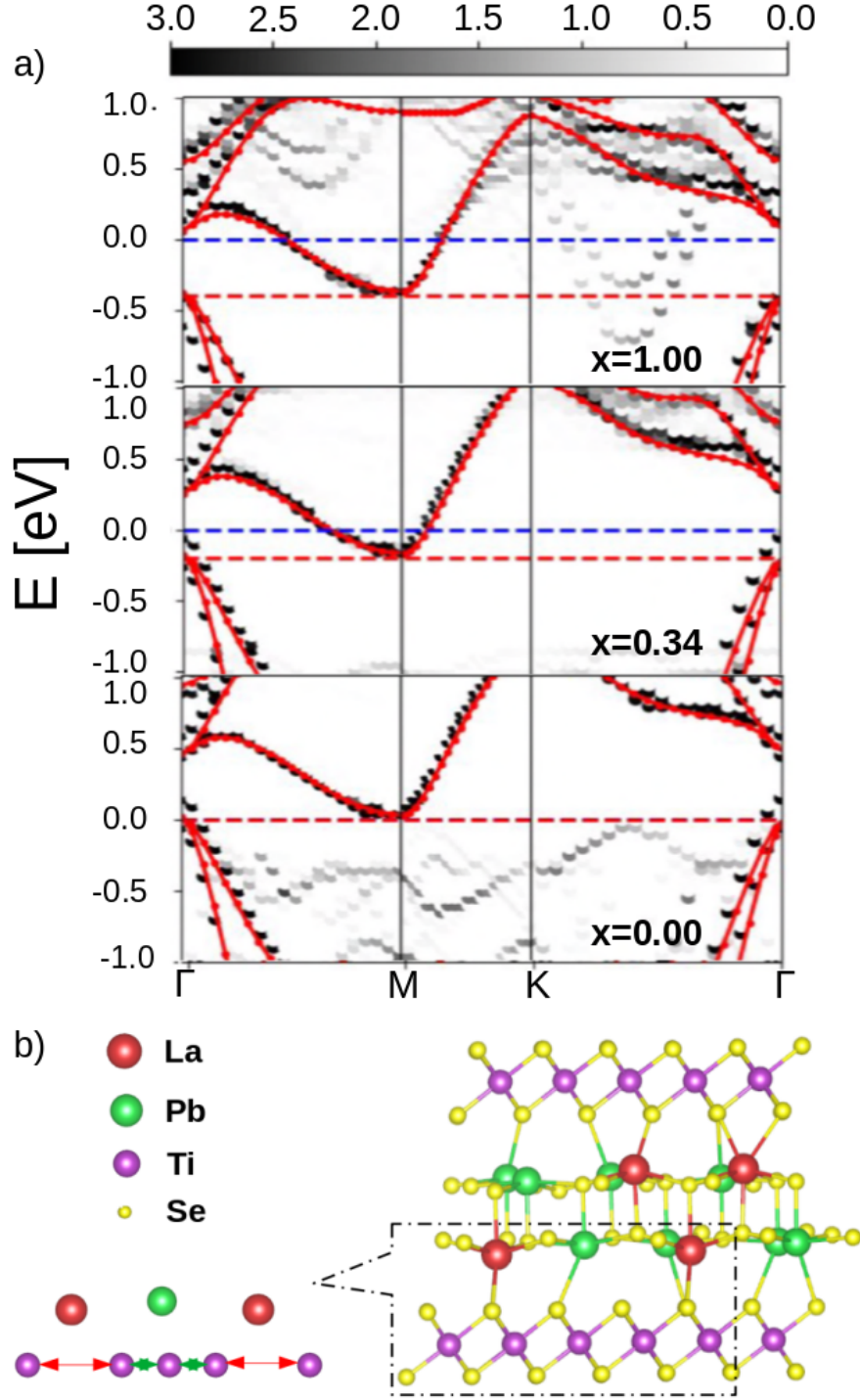


Figure 4: a) Band unfolding onto the single layer TiSe_2 Brillouin zone of the misfit compound $(\text{La}_x\text{Pb}_{1-x}\text{Se})_{1.18}(\text{TiSe}_2)_2$ for $x = 1.0, 0.34, 0.0$. The band structure for the isolated single layer TiSe_2 (red line) is superimposed and aligned to the bottom of the Ti d-band in the misfit. The blue dashed line corresponds to the Fermi level E_F of the misfit compound, while the red one to the Fermi level of the isolated TiSe_2 layer (in the lowest panel they coincide). b) Lattice deformation of the TiSe_2 layers generated by the partial substitution of Pb atoms in $(\text{La}_x\text{Pb}_{1-x}\text{Se})_{1.18}(\text{TiSe}_2)_2$. The magnified portion shows a bond length alternation in the TiSe_2 lattice with two different distances d_1 (red) and d_2 (green).

misfit in such a way that the doping level is rigidly adjustable through appropriate alloying of the RS Q-layer.

For this reason we consider MLCs having the following stoichiometry $(\text{La}_x\text{Pb}_{1-x}\text{Se})_{1.18}(\text{TiSe}_2)$ as a function of x . We point out that similar substitutions ($\text{La} \leftrightarrow \text{Sr}$) have already been achieved in sulfur-based MLC.¹⁸ A comparison between this system and the previous results for the NbSe_2 series will allow us to draw conclusions that are less dependent on the chosen TMD.

From the previous reasoning and from Fig. 2, we expect that the La concentration (x) allows to tune the carrier concentration in the TiSe_2 layers with $x = 1$ ($x = 0$) corresponding to the highest (lowest) n-doping. In Fig.[4] we show the calculated band structure of the full $(\text{La}_x\text{Pb}_{1-x}\text{Se})_{1.18}(\text{TiSe}_2)_2$ misfit for $x = 1.0, 0.34, 0.0$. We also plot (red continuous line) the electronic structure for an isolated single layer. The position of the bottom of the Ti d-band of the isolated single layer is aligned to the corresponding band in the misfit. As it can be seen, by increasing x the doping is increased. Most important, the Ti d-band displays no deformation upon doping. At the highest doping level ($x = 1$, corresponding to a charge transfer of 0.53 electrons per Ti, which is $n_e \sim 5 \times 10^{14} \text{ e}^- \text{ cm}^{-2}$) two parabolic La bands cross the Fermi level along the ΓK direction. These bands disappear by decreasing x (see SI for calculation at additional values of x). Remarkably, the electronic structure of $(\text{PbSe})_{1.18}(\text{TiSe}_2)_2$ is almost indistinguishable from the one of the isolated TiSe_2 layer.

Despite this similarity in the electronic structure, we find that $(\text{PbSe})_{1.18}(\text{TiSe}_2)_2$ does not display a 2×2 CDW as it happens in the case of the supported TiSe_2 single layer.²²⁻²⁴ This result is in agreement with resistivity data on this MLC⁷ where no CDW was detected. We attribute the suppression of the CDW to the strong bonding between TiSe_2 and the the RS Q-layer. We find that in $(\text{La}_x\text{Pb}_{1-x}\text{Se})_{1.18}(\text{TiSe}_2)_2$, for $x \neq 0, 1$, the Ti-Ti distances are modulated by the presence of Pb atoms in the host LaSe lattice (i.e. the Ti-Ti distance becomes shorter if the Ti atoms are close to a Pb atom). The reason is mostly sterical as the La atomic radius is larger than the one of Pb, therefore Pb atoms are more strongly

bounded to the RS layer and a consequent deformation of the LaSe rocksalt host occurs (as shown in Fig. 4 (b)) followed by a modulation of the Ti-Ti distances. We verified that even starting from 2×2 distorted TiSe_2 layers in the misfit, the structural optimization suppresses the CDW and leads to other distortion patterns that essentially follow the Pb atoms superstructure. Our analysis shows that altering the chemical composition of the rocksalt has a double effect: on the one hand, it allows to precisely tune the rigid doping of the TMD, on the other hand it suppresses the 2×2 CDW of the TiSe_2 bilayer and introduces an additional modulation related to the alternation of La and Pb.

After achieving a complete knowledge of the charge transfer in MLC, we now demonstrate how to design a misfit superconductor starting from its constituents. In particular we show that non-superconducting pristine RS and TMD compounds can lead to a superconductor via charge transfer control (emergent superconductivity).

We consider the layered indirect gap semiconductor $1\text{T}\text{SnSe}_2$ that can be exfoliated and synthesized in single layer form.²⁵ The electronic structure of a single layer SnSe_2 is shown in Fig. 5 (red line). The conduction band is formed by an isolated band with a Van Hove singularity point at K. A maximum in the density of states occurs at the energy corresponding to the band flattening. If the Fermi level is tuned at the inflection point, this would be beneficial for superconductivity. However, this involves a ≈ 1.4 eV Fermi level shift corresponding to a charge transfer of 0.77 electrons ($\approx 6 \times 10^{14} \text{e}^- \text{cm}^{-2}$), unreachable even in a ionic-liquid based field effect transistor. However, as previously shown, this electron doping level could be reached in the misfit $(\text{La}_x\text{Pb}_{1-x}\text{Se})_{1.27}(\text{SnSe}_2)_2$. In order to confirm this hypothesis, we perform first principles calculations for this MLC as a function of x (see Fig. 8 in SI). We find that the La-Pb alloying allows a perfect control of the doping level due to the large work function difference between LaSe and SnSe_2 and an insulator-to-metal transition occurs in SnSe_2 . At $x = 1.00$ the Fermi level perfectly matches the inflection point, as shown in Fig. 5. It is worth noting that at this high La concentration, some LaSe bands cross the Fermi level close to the K point and along ΓK , however their contribution

to the total density of states is marginal. In Fig. 5 we also compare the MLC surface electronic structure with the one of an isolated layer (red line). As it can be seen, there is a substantial band distortion with respect to the isolated single layer. A better description of the surface electronic structure is obtained by replacing the LaSe layer with a uniformly positive charged potential barrier, as in a single gate field effect transistor setup by using the method developed in Ref. ²⁶ The electronic structure of an isolated SnSe₂ layer under this approximation is the green line in Fig. 5, in perfect agreement with the complete calculation of the MLC surface electronic structure both for what concerns the band bending at the Fermi level (some deviations are seen in the empty states close to zone center) and for the position of the valence band top. We attribute the band-bending occurring at the K high-symmetry point to a modification of the intralayer spacing between Sn and Se in SnSe₂ due to the charging of the monolayer (a table with intralayer spacing comparisons can be found in Fig. 7 of SI).

This result shows that it is possible via Pb/La alloying in the RS layers to set the Fermi level at the Van Hove singularity. Furthermore, it shows that the LaSe Q-layer can be assimilated to a capacitor plate in a Field Effect Transistor (FET) (see Fig. 1(a)). This remains true even for the SnSe₂ bilayers in the bulk of the sample, i.e. the full MLC can be assimilated to several field-effect transistors stacked periodically along the z-axis of the MLC, as shown in Fig. 1.

As superconductivity is a bulk property, we must simulate the complete 3D crystal. The calculation of the vibrational properties and electron-phonon coupling for the complete MLC is, however, a very cumbersome task due to the large number of atoms. We then proceed differently, namely we consider a SnSe₂ bilayer in a field effect configuration as in Fig. 1 with a +0.7 charge on each of the two plates (double gate configuration). In order to prevent the ions from moving too close to the gate electrodes, a potential barrier is placed before the gates, and the total charge of the system is maintained equal to zero.²⁶ Additional details on these calculations can be found in the SI. We have verified that this approach gives geometries

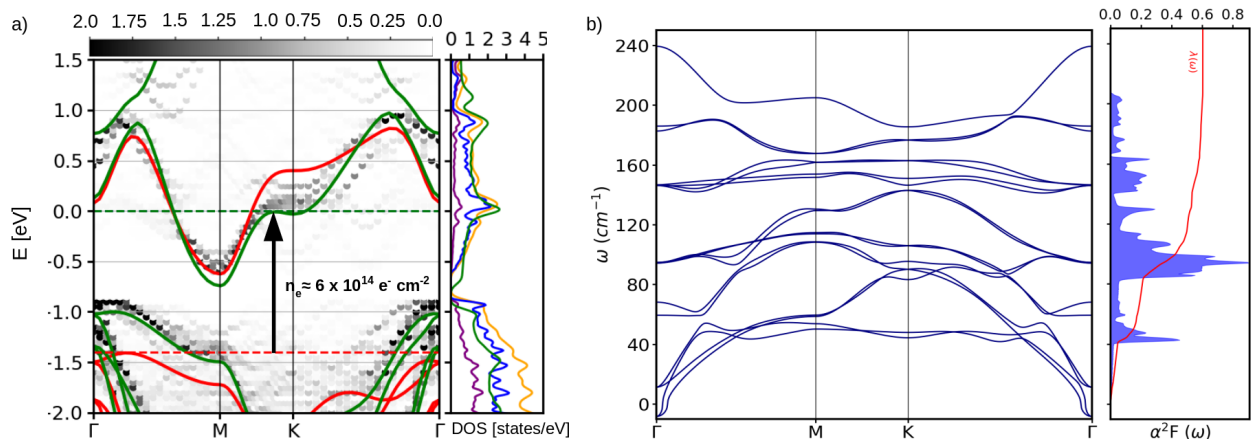


Figure 5: Panel a): band unfolding of $(\text{LaSe})_{1.27}(\text{SnSe}_2)_2$ misfit supercell onto the hexagonal primitive Brillouin Zone (BZ) of single layer SnSe_2 (the zero energy is set to the Fermi level, dashed green line). The superimposed solid lines are the band structure of an isolated single layer SnSe_2 (red), and of a single layer SnSe_2 doped in a single FET setup as in $(\text{LaSe})_{1.27}(\text{SnSe}_2)_2$ by 0.7 electrons per Sn atoms (green), respectively. Darker regions in the colormap represent the most relevant projection of the misfit eigenvalues of the band structure in the SnSe_2 first BZ (band unfolding). In the adjacent panel we plot the total DOS per SnSe_2 formula unit of $(\text{LaSe})_{1.27}(\text{SnSe}_2)_2$ (yellow) and the projected density of states over atomic orbitals of the LaSe layers (purple) and of the SnSe_2 layers (blue), respectively. The green line is the DOS of a single layer SnSe_2 doped in a single FET setup of 0.7 electrons per Sn atoms. Panel b): dynamical properties and electron-phonon coupling of $(\text{LaSe})_{1.27}(\text{SnSe}_2)_2$ modeled by a bilayer SnSe_2 in a double FET setup. The phonon dispersion is shown in the first panel while, in the adjacent panel, the Eliashberg function $\alpha^2 F(\omega)$ (filled blue curve) and the total electron-phonon coupling $\lambda(\omega)$ (red) are depicted.

for the SnSe₂ bilayer in excellent agreement with the complete MLC structural optimization. Furthermore the electronic density of states of the MLC and that of the monolayer in double gate configuration are practically indistinguishable, as shown in Fig. 5.

We then calculate the phonon dispersion ($\omega_{\mathbf{q}\nu}$) and the electron-phonon coupling $\lambda_{\mathbf{q}\nu}$ for each mode ν of phonon crystal momentum \mathbf{q} in double gate geometry. From these quantities we obtain the Eliashberg function $\alpha^2F(\omega) = \frac{1}{2N_q} \sum_{\mathbf{q}\nu} \lambda_{\mathbf{q}\nu} \omega_{\mathbf{q}\nu} \delta(\omega - \omega_{\mathbf{q}\nu})$ and the average electron-phonon coupling $\lambda = \frac{1}{N_q} \sum_{\mathbf{q}\nu} \lambda_{\mathbf{q}\nu} = 0.6$, N_q being the number of points in the phonon momentum grid used to calculate the average (we used a $96 \times 96 \times 1$ \mathbf{q} -grid, see the SI). These quantities are plotted in Fig. 5 (b). Approximately 30% of the coupling arises from the Einstein optical modes at $\approx 45 - 50 \text{ cm}^{-1}$, while the rest of the coupling is uniformly distributed throughout the other modes. The phonon density of states (not shown) is very similar to the Eliashberg function.

We calculate the superconducting critical temperature by solving the anisotropic Migdal-Eliashberg equations,²⁷ as implemented in the EPIq software,^{28,29} and by assuming $\mu^* = 0.1$, obtaining a superconducting critical temperature of $T_c = 3.5 \text{ K}$ (see SI for details on Migdal-Eliashberg calculations). This result matches well with the $T_c = 4.8 \text{ K}$ detected in ultrathin Li-intercalated SnSe₂ via field effect gating and demonstrates that superconductivity can emerge in MLC from pristine components that are not superconducting.

In conclusion, by performing extensive first principles electronic structure calculations on misfit layer compounds we unveiled the mechanism ruling charge transfer in these systems. In particular, due to their large work functions, we showed that TMDs are always acceptors while rocksalts are always donors. The electron density that can be injected in the TMD layers can be as high as $6 \times 10^{14} \text{ e}^- \text{ cm}^{-2}$, sensibly larger than in ordinary field-effect transistors.

We have shown that the charging of the TMD layers can be efficiently controlled via the La \leftrightarrow Pb substitution. Most interesting, by replacing each RS Q-layer with a charged plate and a barrier, we have shown that the surface of the MLC behaves as a single gated

field-effect transistor while the bulk can be seen as a periodic arrangement of double-gated field effect transistor.

Finally and most important, we have shown that from the knowledge of the RS and TMD constituents it is possible to infer the amount of charge transfer to the TMD layers in the MLC and to predict the physical properties of the heterostructure. As a practical demonstration, we showed that emergent superconductivity occurs in $(\text{LaSe})_{1.27}(\text{SnSe}_2)_2$ via a 1.4 eV Fermi level shift induced by the presence RS Q-layers in the misfit. The methodology developed in this work paves the way to the synthesis and design of misfit compounds with tailored physical properties.

Acknowledgements

We acknowledge EuroHPC for awarding us access to the LUMI supercomputer (grant number 465000468). We acknowledge support from the European Union’s Horizon 2020 research and innovation programme Graphene Flagship under grant agreement No 881603.

Supporting Information

Contains:

- I. Geometrical Details of MLCs.
- II. Technical details.
- III. Band Alignment Calculation.
- IV. Band unfolding method applied to $(\text{La}_x\text{Pb}_{1-x}\text{Se})_{1.18}(\text{TiSe}_2)_2$.
- V. Doping-induced Superconductivity.

References

- (1) Wu, Y.; Li, D.; Wu, C.-L.; Hwang, H. Y.; Cui, Y. Electrostatic gating and intercalation in 2D materials. *Nature Reviews Materials* **2023**, *8*, 41–53.
- (2) Xi, X.; Berger, H.; Forró, L.; Shan, J.; Mak, K. F. Gate Tuning of Electronic Phase Transitions in Two-Dimensional NbSe₂. *Phys. Rev. Lett.* **2016**, *117*, 106801.
- (3) Leriche, R. T. et al. Misfit Layer Compounds: A Platform for Heavily Doped 2D Transition Metal Dichalcogenides. *Advanced Functional Materials* **2021**, *31*, 2007706.
- (4) Wiegiers, G. Misfit layer compounds: Structures and physical properties. *Progress in Solid State Chemistry* **1996**, *24*, 1–139.
- (5) Rouxel, J.; Meerschaut, A.; Wiegiers, G. Chalcogenide misfit layer compounds. *Journal of Alloys and Compounds* **1995**, *229*, 144–157.
- (6) Samuely, P.; Szabó, P.; Kačmarčík, J.; Meerschaut, A.; Cario, L.; Jansen, A. G. M.; Cren, T.; Kuzmiak, M.; Šofranko, O.; Samuely, T. Extreme in-plane upper critical magnetic fields of heavily doped quasi-two-dimensional transition metal dichalcogenides. *Phys. Rev. B* **2021**, *104*, 224507.
- (7) Giang, N.; Xu, Q.; Hor, Y. S.; Williams, A. J.; Dutton, S. E.; Zandbergen, H. W.; Cava, R. J. Superconductivity at 2.3 K in the misfit compound (PbSe)_{1.16}(TiSe₂)₂. *Phys. Rev. B* **2010**, *82*, 024503.
- (8) Kim, J. H.; Yun, J. H.; Song, Y. J.; Rhyee, J.-S. Anisotropic thermoelectric and superconducting properties of the bulk misfit-layered (SnSe)_{1.17}(TaSe₂) compound. *Current Applied Physics* **2021**, *28*, 1–6.
- (9) Šofranko, O.; Leriche, R.; Morales, A.; Cren, T.; Sasaki, S.; Cario, L.; Szabo, P.; Samuely, P.; Samuely, T. Periodic Surface Modulation of (LaSe)_{1.14}(NbSe₂) Observed by Scanning Tunneling Microscopy. *Acta Physica Polonica A* **2020**, *137*, 785–787.

- (10) Yang, X.; Ma, J.; Lv, B.; Hu, H.; Sun, T.; Li, M.; Qiao, L.; Wu, S.; Tao, Q.; Cao, G.-H.; Xu, Z.-A. Enhanced superconductivity in a misfit compound $(\text{PbSe})_{1.12}(\text{TaSe}_2)_2$ with double TaSe_2 layers. *Europhysics Letters* **2019**, *128*, 17004.
- (11) Grosse, C.; Alemayehu, M. B.; Falmbigl, M.; Mogilatenko, A.; Chiatti, O.; Johnson, D. C.; Fischer, S. F. Superconducting ferecrystals: turbostratically disordered atomic-scale layered $(\text{PbSe})_{1.14}(\text{NbSe}_2)_n$ thin films. *Scientific Reports* **2016**, *6*, 33457.
- (12) Atkins, R.; Disch, S.; Jones, Z.; Haeusler, I.; Grosse, C.; Fischer, S. F.; Neumann, W.; Zschack, P.; Johnson, D. C. Synthesis, structure and electrical properties of a new tin vanadium selenide. *Journal of Solid State Chemistry* **2013**, *202*, 128–133.
- (13) Trump, B. A.; Livi, K. J.; McQueen, T. M. The new misfit compound $(\text{BiSe})_{1.15}(\text{TiSe}_2)_2$ and the role of dimensionality in the $\text{Cu}_x(\text{BiSe})_{1+\delta}(\text{TiSe}_2)_n$ series. *Journal of Solid State Chemistry* **2014**, *209*, 6–12.
- (14) Falmbigl, M.; Putzky, D.; Ditto, J.; Johnson, D. Influence of interstitial V on structure and properties of ferecrystalline $([\text{SnSe}]_{1.15})_1(\text{V}_{1+x}\text{Se}_2)_n$ for $n=1, 2, 3, 4, 5$, and 6 . *Journal of Solid State Chemistry* **2015**, *231*, 101–107.
- (15) Göhler, F.; Ramasubramanian, S.; Rajak, S. K.; Rösch, N.; Schütze, A.; Wolff, S.; Cordova, D. L. M.; Johnson, D. C.; Seyller, T. Modulation doping and charge density wave transition in layered PbSe-VSe_2 ferecrystal heterostructures. *Nanoscale* **2022**, *14*, 10143–10154.
- (16) Pei, C. et al. Pressure-Induced Superconductivity in Topological Heterostructure $(\text{PbSe})_5(\text{Bi}_2\text{Se}_3)_6$. 2023; <https://arxiv.org/abs/2301.01120>.
- (17) Luo, H.; Yan, K.; Pletikosic, I.; Xie, W.; Phelan, B. F.; Valla, T.; Cava, R. J. Superconductivity in a Misfit Phase That Combines the Topological Crystalline Insulator $\text{Pb}_{1-x}\text{Sn}_x\text{Se}$ with the CDW-Bearing Transition Metal Dichalcogenide TiSe_2 . *Journal of the Physical Society of Japan* **2016**, *85*, 064705.

- (18) Cario, L.; Johrendt, D.; Lafond, A.; Felser, C.; Meerschaut, A.; Rouxel, J. Stability and charge transfer in the misfit compound $(\text{LaS})(\text{SrS})_{0.2}\text{CrS}_2$: Ab initio band-structure calculations. *Phys. Rev. B* **1997**, *55*, 9409–9414.
- (19) Kim, H.-g.; Choi, H. J. Thickness dependence of work function, ionization energy, and electron affinity of Mo and W dichalcogenides from DFT and GW calculations. *Phys. Rev. B* **2021**, *103*, 085404.
- (20) Giannozzi, P.; Baseggio, O.; Bonfà, P.; Brunato, D.; Car, R.; Carnimeo, I.; Cavazzoni, C.; de Gironcoli, S.; Delugas, P.; Ferrari Ruffino, F.; Ferretti, A.; Marzari, N.; Timrov, I.; Urru, A.; Baroni, S. Quantum ESPRESSO toward the exascale. *The Journal of Chemical Physics* **2020**, *152*, 154105.
- (21) Perdew, J. P.; Burke, K.; Ernzerhof, M. Generalized Gradient Approximation Made Simple. *Physical Review Letters* **1996**, *77*, 3865–3868.
- (22) Kolekar, S.; Bonilla, M.; Ma, Y.; Diaz, H. C.; Batzill, M. Layer- and substrate-dependent charge density wave criticality in 1T-TiSe₂. *2D Materials* **2018**, *5*, 015006.
- (23) Wang, H.; Chen, Y.; Duchamp, M.; Zeng, Q.; Wang, X.; Tsang, S. H.; Li, H.; Jing, L.; Yu, T.; Teo, E. H. T.; Liu, Z. Large-Area Atomic Layers of the Charge-Density-Wave Conductor TiSe₂. *Advanced Materials* **2018**, *30*, 1704382.
- (24) Fang, X.-Y.; Hong, H.; Chen, P.; Chiang, T.-C. X-ray study of the charge-density-wave transition in single-layer TiSe₂. *Phys. Rev. B* **2017**, *95*, 201409.
- (25) Fu, J.; Zhao, L.; Zhou, L.; Wu, K.; Du, J.; Wang, X.; Song, J.; Zhu, L.; Zhou, F.; Huan, Y.; Bao, L.; Wang, R.; Zhang, Q.; Zhang, Y. Controllable Synthesis of Atomically Thin 1T-SnSe₂ Flakes and Its Linear Second Harmonic Generation with Layer Thickness. *Advanced Materials Interfaces* **2022**, *9*, 2102376.

- (26) Sohler, T.; Calandra, M.; Mauri, F. Density functional perturbation theory for gated two-dimensional heterostructures: Theoretical developments and application to flexural phonons in graphene. *Phys. Rev. B* **2017**, *96*, 075448.
- (27) Allen, P. B.; Mitrović, B. In *Theory of Superconducting T_c* ; Ehrenreich, H., Seitz, F., Turnbull, D., Eds.; Solid State Physics; Academic Press, 1983; Vol. 37; pp 1–92.
- (28) Marini, G.; Calandra, M. Phonon mediated superconductivity in field-effect doped molybdenum dichalcogenides. *2D Materials* **2022**, *10*, 015013.
- (29) Calandra, M.; Profeta, G.; Mauri, F. Adiabatic and nonadiabatic phonon dispersion in a Wannier function approach. *Phys. Rev. B* **2010**, *82*, 165111.